Nano Energy 53 (2018) 83–90

Contents lists available at ScienceDirect

Nano Energy

journal homepage: www.elsevier.com/locate/nanoen

Full paper

Firmly standing three-dimensional radial junctions on soft aluminum foils enable extremely low cost flexible thin film solar cells with very high power-to-weight performance

Xiaolin Sun[a,b], Ting Zhang[a], Junzhuan Wang[a,*], Fan Yang[a], Ling Xu[a], Jun Xu[a], Yi Shi[a], Kunji Chen[a], Pere Roca i Cabarrocas[c], Linwei Yu[a,c,**]

[a] National Laboratory of Solid State Microstructures/School of Electronics Science and Engineering/Collaborative Innovation Center of Advanced Microstructures, Nanjing University, 210093 Nanjing, PR China
[b] Institute of Electronics Information Engineering, Sanjiang University, 210012 Nanjing, PR China
[c] LPICM, CNRS, Ecole Polytechnique, Université Paris-Saclay, 91128 Palaiseau, France

ARTICLE INFO

Keywords:
Flexible photovoltaics
Silicon nanowires
Radial p-i-n junction
Thin film solar cells
Power-to-weight ratio
Aluminum foil

ABSTRACT

Flexibility and power-to-weight (PTW) ratio are the key factors for promoting wearable or portable solar cell applications. Planar hydrogenated amorphous silicon (a-Si:H) thin films deposited directly on soft aluminum foils (AF) are usually subject to easy cracking and delamination due to the mechanical instability on AF surface. Here, an exceptionally robust three-dimensional (3D) construction of a-Si:H radial p-i-n junction solar cells on soft supermarket-available AF of 15 μm thick is reported, where the discrete and firmly standing Si nanowire (SiNW) cores, grown and rooted on the soft AF surface, frame up a 3D architecture that protects the protrusive photo-active radial junctions from the unstable a-Si/Al bottom layer. An excellent flexibility and integrity of the 3D a-Si:H radial junctions have been achieved, even under bending to radius of 5 mm. Remarkably, without any diffusion barrier protection, a power conversion efficiency of 5.6% has been recorded, with an open-circuit voltage of 0.71 V and photo-current density of 14.2 mA/cm^2, leading to a high PTW ratio of > 1300 W/kg. Importantly, the overall fabrication cost can be largely slashed off, by ~46% compared to conventional a-Si:H solar cells, as the need for a bottom TCO contact/texturing layer, for a back-reflection coating and for a glass/polymer substrate are all exempted.

1. Introduction

Flexible and light-weight solar cells are finding broad applications in portable and wearable electronics, where the power-to-weight (PTW) ratio is a critical parameter for implementation [1–7]. Compared to the flexible solar cells built on organic, hybrid perovskite materials [8–11] or ultra-thin mono crystalline silicon wafers (thickness < 40 μm, thinned by chemical etching or exfoliation) [12,13], hydrogenated amorphous silicon (a-Si:H) thin film solar cells can be made via a low-cost, large scale and industrial-proven mature technology, without the use of any toxic or heavy-metal elements [14,15], while boasting still a better weak light performance [16] and a lower temperature coefficient [17,18]. Usually, flexible a-Si:H solar cells are constructed upon stainless steel (SS) [16,19–21] or PI (polyimide) and PEN (polyethylene naphthalate) polymer substrates [4,5,16,22], where transparent conductive oxide (TCO) texturing, back-reflection coating and nickel/or chromium diffusion barrier layers are required to enhance light harvesting and, more importantly, to prevent metal diffusion from the bottom substrate into the p-i-n junctions [4,19,21–23]. However, all these extra protection and buffer layers add to the fabrication complexity, cost and weight that reduce the PTW ratio performance of flexible thin film modules, which is however becoming a critical figure-of-merit for many portable solar power solutions.

Aluminum foil (AF) has been best known for its high electric conductivity, low cost, excellent optical reflectivity over a wide spectrum of wavelengths, and its outstanding flexibility and self-sustainability even when the AF is thinned to below < 20 μm. However, the surface of the AF substrates is relatively *soft* and mechanically unstable,

* Corresponding author.
** Corresponding author at: National Laboratory of Solid State Microstructures/School of Electronics Science and Engineering/Collaborative Innovation Center of Advanced Microstructures, Nanjing University, 210093 Nanjing, PR China.
E-mail addresses: wangjz@nju.edu.cn (J. Wang), yulinwei@nju.edu.cn (L. Yu).

https://doi.org/10.1016/j.nanoen.2018.08.038
Received 28 April 2018; Received in revised form 17 August 2018; Accepted 17 August 2018
Available online 21 August 2018

compared to those of rigid SS or glass substrates coated with TCO layers [24,25]. As a consequence, a-Si:H thin films deposited over the pliable AF substrates are vulnerable to cracking and even delamination [26,27]. It has also been known that Al atoms can diffuse into the Si thin film, at elevated temperature > 200 °C, to weaken n-type doping in case of contacting an n-type doped a-Si:H layer [4]. Recent works have demonstrated nanostructured anodized aluminum oxide (AAO) patterns [28,29] formed on a thick Al sheet (> 250 μm) as a photonic template to maximize the light absorption performance of a-Si:H solar cells, the needs of extra TCO and metal buffer layers reduce greatly the overall flexibility of the solar cells, while degrading also their PTW ratio performance.

Recently, three-dimensional (3D) silicon nanowires (SiNWs) [30–33] and ZnO nanorods [22,34–37] have been widely explored as a promising architecture towards high performance thin film photovoltaics, where a strong light harvesting performance allows for the use of a thinner intrinsic absorber layer (< 100 nm) that helps to enhance the sweeping built-in field, facilitate carrier collection, suppress light-induced-degradation (LID) effect and tolerate more defective i-layer material [38,39]. All these benefits have been indeed verified in our previous works on the 3D radial junction (RJ) thin film solar cells, constructed over SiNWs grown with tin (Sn) droplets via a vapor-liquid-solid (VLS) process upon rigid TCO-coated glass substrates [40–43]. However, the mechanical advantages and potential of the RJ construction, which could lend themselves to addressing the mechanical challenges at microscale, as illustrated in Fig. 1f, has been little explored.

In this work, we report an exceptionally robust and very low-cost 3D construction of RJ a-Si:H thin-film solar cells over SiNWs directly grown upon supermarket-available, ultra-thin and flexible AF of only 15 μm thick. An excellent flexibility and mechanical stability have been witnessed even under repetitive concave or convex bendings to large curvature of 1/5 mm^{-1}, with still reasonable photoelectric performance under standard AM 1.5G illumination. This also leads to a record high PTW ratio of > 1300 W/kg, thanks to the use of an ultra-thin and light-weight AF as substrate, and exempting the needs for bottom TCO contact/texturing, diffusion barrier and back-reflection layers commonly used in conventional planar solar cells. Further finite element modeling and analysis reveal that the discrete SiNWs, firmly standing and rooted on the soft AF surface, can provide strong anchor-sites to maintain the integrity of the a-Si:H thin films, while the photo-active protrusive RJ regions are well protected from the bottom strain layer.

2. Experimental section

2.1. Device fabrication

The fabrication procedures of the a-Si:H radial junction units are schematically illustrated in Fig. 1a-c, where a thin tin (Sn) layer of 2 nm thick was first evaporated to the surface of aluminum foils (AF, 8011/O of 15 μm thick, as seen for example in the photograph shown in Fig. 1d) purchased from supermarket. Then, the AF pieces were cleaned by ultrasonication in acetone, methanol and deionized water, before being wrapped around glass or wafer holders of one-inch wide to facilitate sample handling. Then, the Sn layer was treated by H_2 plasma in a plasma-enhanced chemical vapor deposition (PECVD) system, with H_2 flow, RF power density and chamber pressure of 20 standard cubic centimeter per minute (SCCM), 10 mW/cm^2 and 30 Pa at 200 °C, respectively, for 5 min to form discrete Sn droplets that were later used as catalyst to mediate the vertical growth of SiNWs, via a plasma enhanced VLS process with silane (SiH_4) as precursor at 400 °C. During the VLS growth, a mixture of 60 SCCM H_2, 6 SCCM silane (SiH_4) and 2.2 SCCM diborane dopant (B_2H_6) precursor gases was introduced to grow vertical p-type SiNWs directly upon the AF surface, with a RF power density and chamber pressure of 20 mW/cm^2 and 130 Pa for 15 min. Note that the SiNWs feature, as seen for example in the top and side-view SEM images in Fig. 1e-f, a typical length of 1 μm and a gradually tapering diameter from 50 nm at the root to 20 nm at the tip. In the next step, intrinsic and n-type a-Si:H layers, of around 80 nm and 10 nm thick on the sidewall, were subsequently deposited around the SiNW cores at 150 °C, without or with 2.3 SCCM phosphine (PH_3) dopant gas, respectively. Finally, an ITO layer was deposited around the RJ units by magnetron sputtering to serve as the top transparent electrode. A

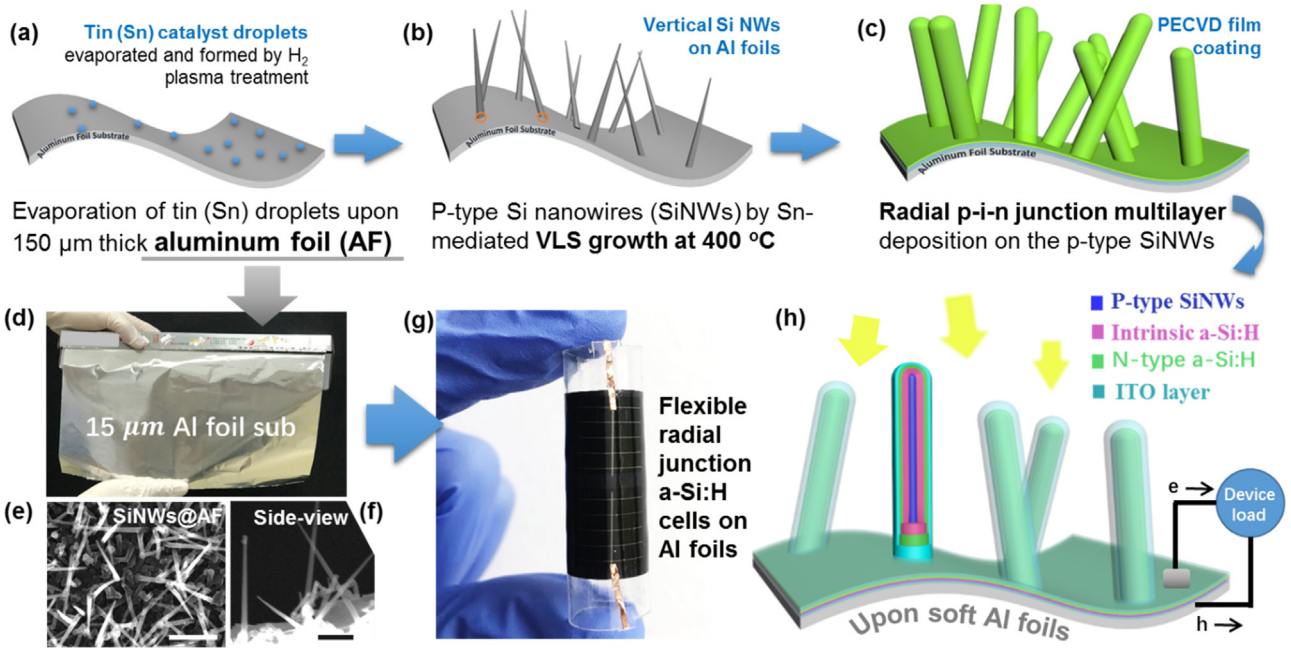

Fig. 1. (a-c) illustrate the fabrication procedures of the a-Si:H radial junctions standing directly upon the soft surface of the 15 μm thick supermarket-available flexible AF, with a photo shown in (d). (e-f) present the top and side-viewed SEM images of the SiNWs grown directly on the AF, where the scale bars are for 400 nm and 200 nm, respectively. (g) shows a photo of the final radial junction solar cells on AF, encapsulated in EVA polymer layers. (h) depicts a cross-section view of the inner co-axial p-i-n multilayer structure of the radial junction units.

schematic sketch of the complete RJ structures is presented in Fig. 1h, revealing the cross section of the multilayer profile within a RJ unit. When the light is shed in from top, photo-carriers are generated in the RJ units and collected by the top ITO and the bottom SiNW/AF electrodes, as depicted schematically in Fig. 1h.

2.2. Device characterizations

The *J-V* characteristics were measured under standard AM1.5G illumination (Newport, Oriel Sol-1A), while the EQE responses were measured by QEX-10 measurement System, with a wavelength scan range from 300 nm to 800 nm with a sweep step of 10 nm.

2.3. Encapsulation

The samples were encapsulated within ethylene-vinyl acetate copolymer (EVA) at lamination temperature of 145 ℃, where piecewise pressing was applied, with pressure and duration of 0.2 Pa and 2 min and 0.8 Pa for 8 min, respectively. The photo-current extraction electrodes are formed by rolled copper foil tapes, which were first glued to the anodes and the cathodes of the RJ solar cells, as shown in Fig. 1g, and then encapsulated in EVA thin films by using the standard process in *Trina Solar Ltd.* with the encapsulation parameters as described above.

3. Results and discussions

Fig. 2a shows a typical side-view SEM image of a dense array of RJs grown over a large area upon the AF surface. The distribution of the RJ array is found to be rather uniform, despite of the curved surface and random stripes, with typical fluctuations of 1–3 μm as marked by the dashed white lines, which are very common for commercial AF due to the standard twin-roll-casting process [44]. A comparison of the RJ and planar a-Si:H p-i-n junction thin films deposited directly on AF surface is presented in Fig. 2c and d, respectively, where the microscope photographs show that the planar a-Si:H thin films on the AF are extremely vulnerable to even slight bending of AF, leaving large cracks and peeling off segments (Fig. 2c), while the SiNW-supported RJ thin film is found to be rather continuous and uniform (Fig. 2d). This finding provides, first of all, a strong proof of the outstanding mechanical stability and robustness of the 3D RJ thin film construction to accommodate the large surface roughness and fluctuations upon the mechanically unstable soft AF surface.

A closer top-view SEM image of the RJ structure is presented in the inset of Fig. 2a, where the RJ units, of ~180 nm in diameter (without ITO) and ~1 μm long, are randomly oriented. A comparison of the RJ units, before and after ITO coating, is provided in the cross-section SEM images shown in Fig. 2b. It is interesting to note that, while the a-Si:H thin film coating by PECVD can be quite conformal around the SiNWs, the deposition of ITO by sputtering is not so uniform, especially along the depth of standing RJ units. For instance, while the RJ has a rather uniform diameter of ~200 nm, the ITO coating thickness varies from 100 nm on the top to only 40 nm at the root and on the bottom surface. This is seemingly a disadvantage for photo-current collection along the bottom ITO pathway (BIP) that is thinner and thus more resistive. However, among the random but mutually crossed RJ units, there exist

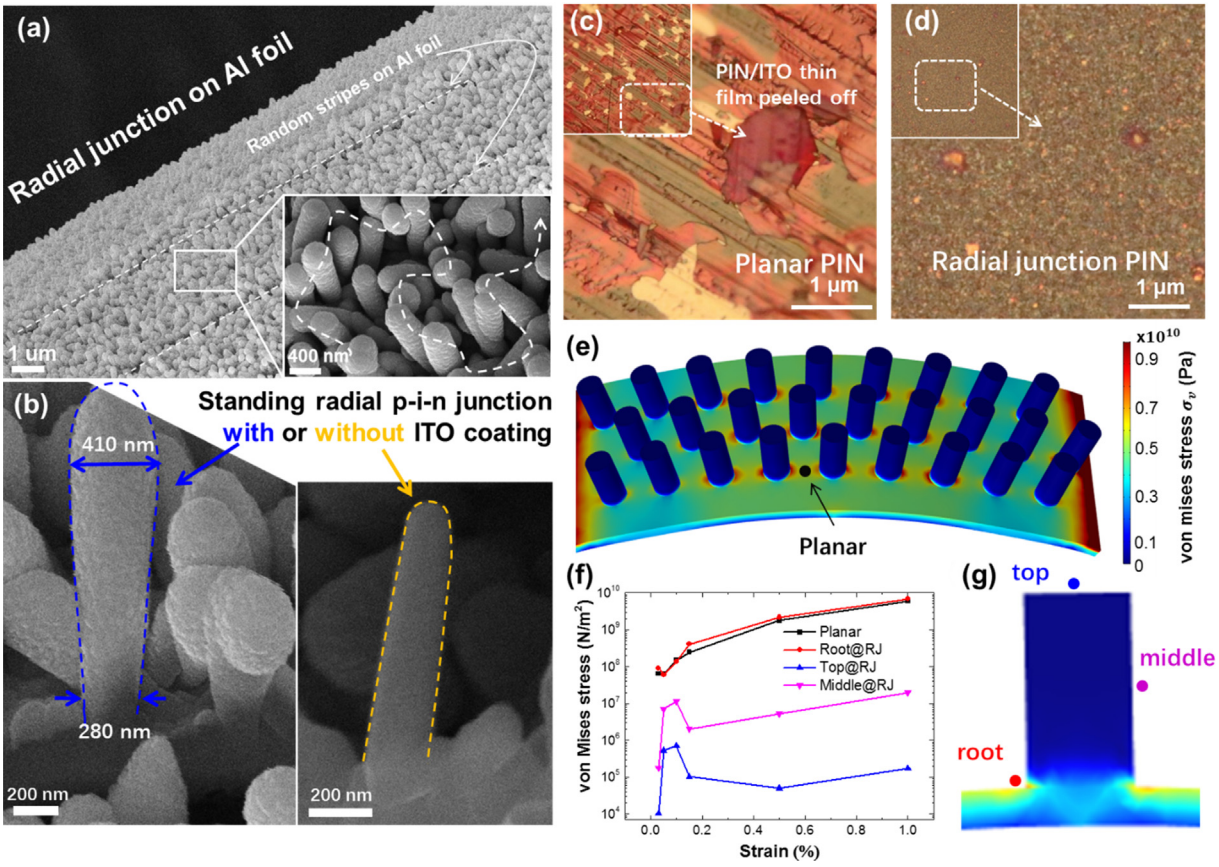

Fig. 2. (a) Side-view SEM image of the a-Si:H RJ thin films grown upon SiNW array standing upon AF surface, while the inset shows more details of the geometric features. Cross-section SEM examinations of the standing RJ units on the soft AF surface, with or without ITO layer, are provided in (b). (c,d) show the microscope photos of the planar and the radial junction thin film structure grown upon the same AF substrate, respectively. The simulated von Mises stress distribution among the RJ units on top of AF substrates, when subject to convex bending, is presented in (e), while the stresses evolutions at three different locations, as marked in (g) and under different bending strains, are extracted and plotted in (f).

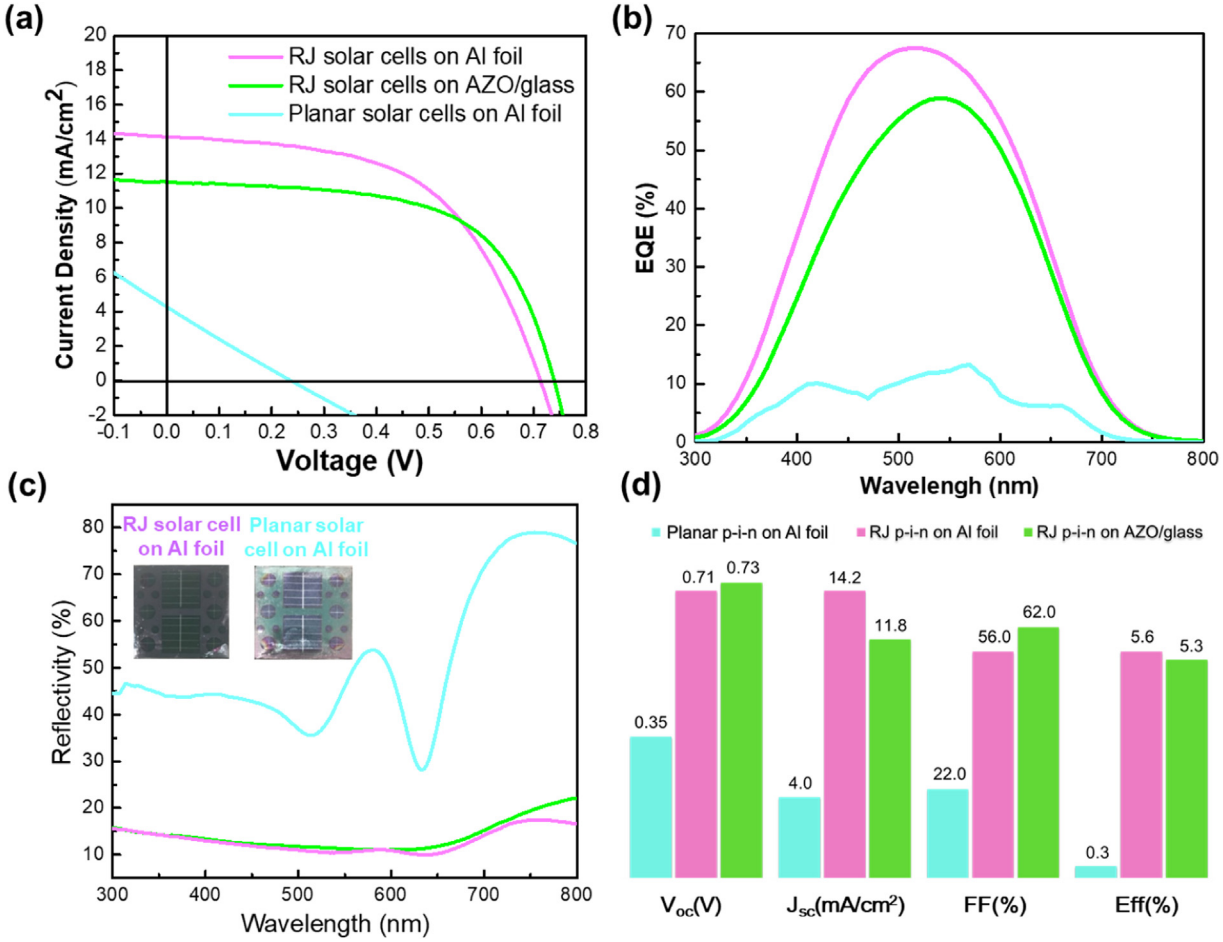

Fig. 3. (a,b) show the current density-voltage (*J-V*) and external quantum efficiency (EQE) curves, measured under AM1.5G illumination for the thin film solar cells in radial junction or planar architectures and upon soft AF or solid AZO glass substrates, with their corresponding performance parameters extracted and compared in the histograms shown in (d). The reflectivity of the three different samples is presented in (c), with the pictures of the RJ and planar thin film solar cells shown in the insets.

also extra current paths, that is the top ITO-crossing pathway (TIP), which can help to transport and collect the photo-current among the crossed RJs. For example, a possible TIP route is marked in the right-bottom inset of Fig. 2a by a white dash line, which is indeed beneficial for the photo-carrier extraction from the 3D-RJ units, without the need to go through the more resistive BIP routes. On the other hand, as demonstrated in our previous simulation works on light field propagation and absorption, most of the incident light will get absorbed by the top portion of the RJ cells. So, the existence of such an extra TIP route for lateral transport can be helpful to extract the photo-current directly from the photo-active regions of the RJs. A poor electric connection to the more defective bottom layers could, to some extent, help to isolate or even suppress the impact from the leakage current sinks usually found at the deep root of RJs. These features are indeed unique in the 3D randomly oriented and crossing RJ framework.

The current density-voltage (*J-V*) measured under standard AM1.5G illumination and the external quantum efficiency (EQE) curves, of the radial junctions on AF, radial junctions on AZO and planar junctions on AF, were measured and presented in Fig. 3a-b, respectively. It is interesting to note that all the radial junction solar cells have achieved a much higher J_{sc} compared to those of planar ones, thanks to a strong light trapping effect among the 3D arrays. This can also be inferred from their reflection spectra presented in Fig. 3c, where the two radial junction samples demonstrate a rather low (10–20%) reflectivity over a wide wavelength range, while the planar junction on AF suffers from a strong reflection, particularly at long wavelengths ($\lambda > 450$ nm). In addition, the radial junctions constructed over AF substrate generate a higher short-circuit photocurrent ($J_{sc} = 14.2$ mA/cm^2) than that by co-deposited radial junctions ($J_{sc} = 11.2$ mA/cm^2) fabricated on flat AZO/glass substrate, which could be partially assigned to the beneficial back-reflection contributed by the AF substrate, while there is no such coating at the bottom for the reference sample on AZO/glass.

Moreover, it is remarkable that, upon the rough and pliable AF, the radial junctions can still deliver an open-circuit voltage of $V_{oc} = 0.71$ V, only slightly lower than that of $V_{oc} = 0.73$ V by the co-deposited radial junctions on flat AZO/glass. In comparison, the planar junctions co-deposited upon the same AF substrate deliver only a rather low $V_{oc} = 0.35$ V, while the planar junctions deposited over AZO/glass can easily achieve an open circuit voltage of $V_{oc} = 0.75$ V (not shown here). These findings highlight the robustness of such 3D-RJ construction, in terms of maintaining the integrity and functionality of the a-Si:H p-i-n thin films deposited over the soft AF surface. Meanwhile, the fill factor (FF) of the RJ cells on AF is only 56%, which is lower than that of 62% for their counterparts on AZO/glass. A possible reason could be that the aluminum oxide layer remaining on the surface of the AF substrate could increase the electric resistance to the RJs. Further improvement is expected given a better surface treatment or complete removal of this oxide layer in further investigations.

The flexibility of the radial junction solar cells fabricated on AF substrate is tested by attaching them to cylinder rods or troughs of different radii, ranging from $R_r = 5$ mm to 25 mm, as shown in Fig. 4a and Fig. 5a, respectively. Note that, though EVA encapsulation can be

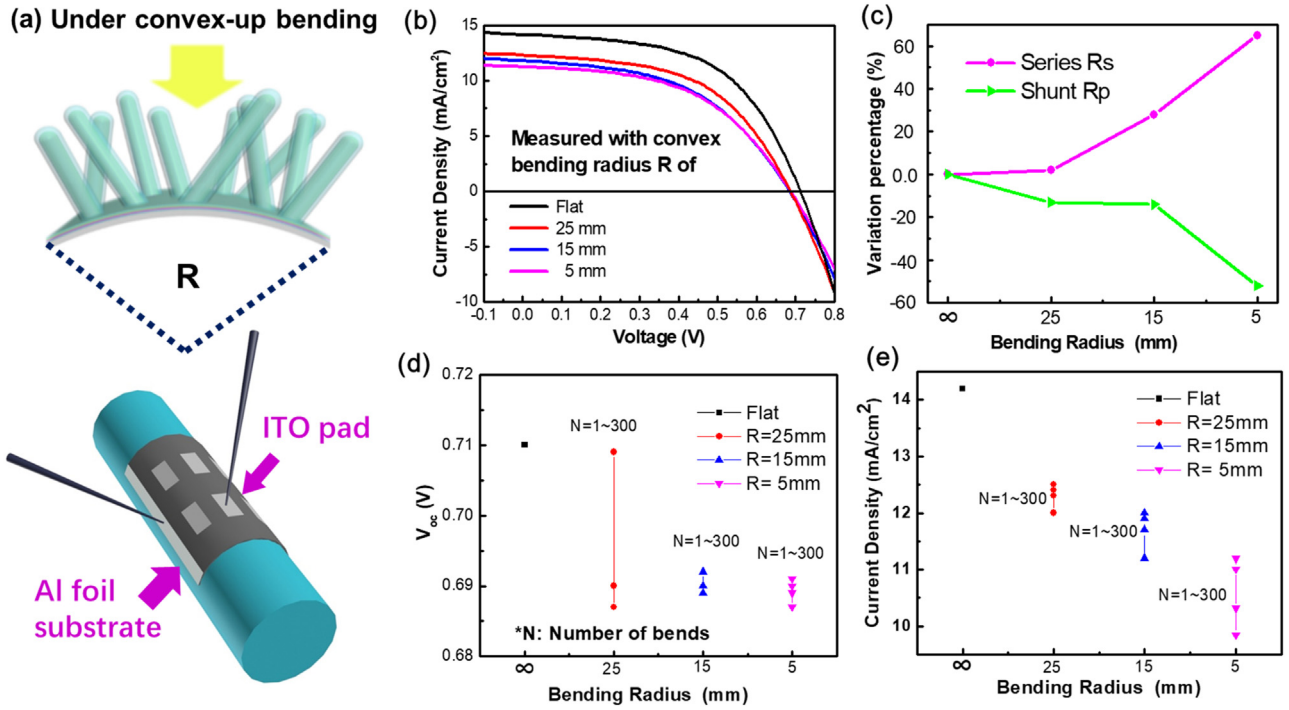

Fig. 4. (a,b) show the convex-up testing photo and *J-V* characteristics with different bending radii. Their corresponding variation trends, in terms of the series and shunt resistances, V_{oc} and J_{sc}, are provided in (c-e), respectively.

applied to encapsulate the radial junctions on AF samples, as seen for example for the one shown in Fig. 1e, the 3D-RJ cells are by themselves robust and self-sustainable enough to go through the tests without the support of EVA layers. So, in the following studies, the bare radial junction samples (complete RJs on AF foils with electric connections but no EVA encapsulation) were characterized while being subject to convex-up bending, as illustrated schematically in Fig. 4a. The evolution of the J-V curves, the contact resistances, the V_{oc} and the J_{sc}, under different bending conditions, are presented in Fig. 4(b), (c), (d) and (e), respectively. It is interesting to note that the V_{oc} remains rather stable with a slight drop to 0.69 V, even after 300 times convex-up bending to a very small radius of $R_r = 5$ mm. This is accompanied, however, with a more significant photo-current decrease (Fig. 4e), when the bending becomes larger and with more bending times. The major reason behind can be assigned to the decreased shunt resistance R_p (by 50% under $R_r = 5$ mm bending) and increased series resistance R_s in the RJ units as witnessed in Fig. 4c. These observations indicate that damages happened in the 3D-RJs under large convex-up bending strain. Despite of this, the radial junction solar cells can still maintain a rather stable V_{oc} output and 71% of their initial PCE up to $R_r = 5$ mm bending.

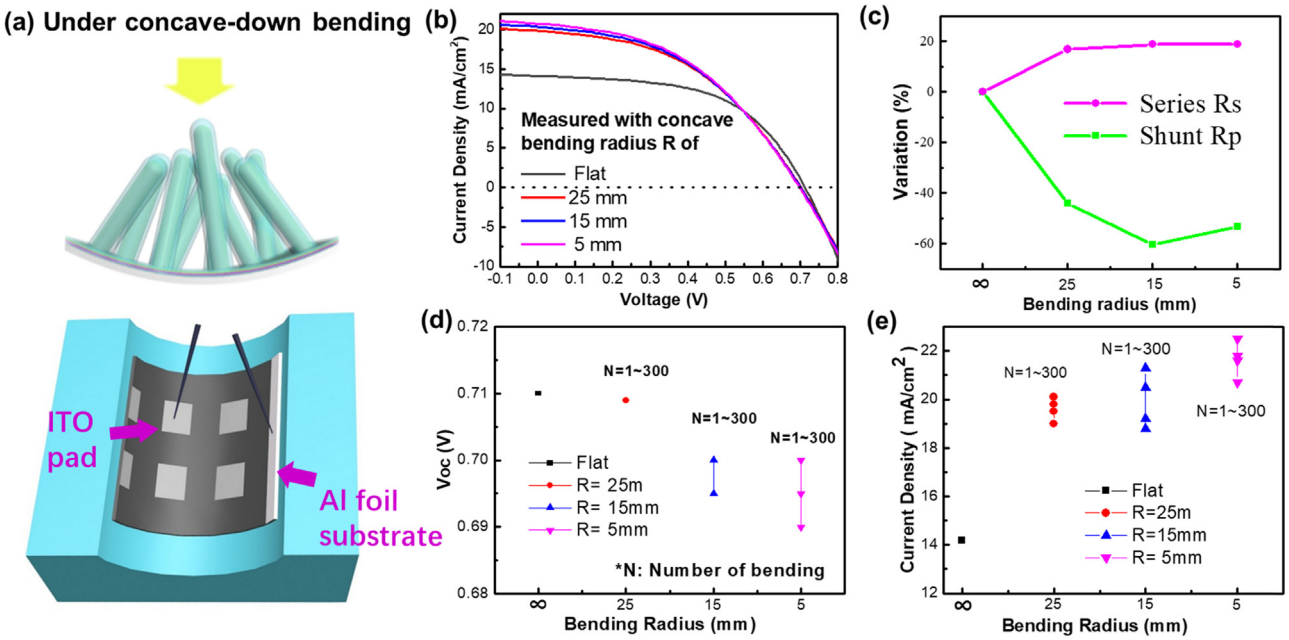

Fig. 5. (a,b) show the concave-down testing photo and *J-V* character with different bending radii, their corresponding variation trends, in terms of the series and shunt resistances, V_{oc} and J_{sc}, are provided in (c-e), respectively.

When the flexible 3D-RJ cell was bent to the opposite direction, that is into a concave-down bending configuration by attaching them to troughs of different radii, as depicted in Fig. 5a, the measured photocurrent density of J_{sc} is found to increase significantly from 14 mA/cm^2 to more than 22 mA/cm^2, as shown in Fig. 5b. Meanwhile, the V_{oc} decreases from 0.71 V to 0.68 V, similar to that observed under convex-up bending. This abnormal J_{sc} increase could arise simply from the fact that the AF substrate in concave bending state plays a role like a mirror that can focus the nearby incident light into the center region, which is equivalent to enhancing the intensity of incident light and thus a higher photocurrent signal can be recorded under concave bending. Meanwhile, it is also interesting to note that, as seen in Fig. 5c, the series resistance R_s extracted under concave bending increases by only 20% (even bent to 5 mm in radius), which is much less significant compared to that of up to 70% in the opposite convex bending as witnessed in Fig. 4c. This can be explained based on a geometry consideration that, among the 3D radial junction architecture, a concave bending will force the nearby radial junction protrusions to lean to their neighbors, and thus forming more extra top-ITO-contacts or TIP routes to counter the increase trend of series resistance under large bending. This is indeed a unique aspect of the 3D mutual-crossed RJ solar cells.

Finite element simulation of the radial junctions constructed upon the flexible AF was also carried out to shed light on the strain distribution among the 3D structures. In Fig. 2e, the edges of a thin AF sheet are fixed while the center is pushed up by a bottom cylinder (hidden for clarity) with different radii. It is clear that, the von Mises stress distribution among the bent 3D radial junctions is not uniform, but mostly concentrated at the roots of the vertical protrusions. The stresses extracted at different distinctive places, as marked in the cross-section profile in Fig. 2g, were plotted against the tensile strain (caused by a convex-up bending) in Fig. 2f. It is found that, while the stresses at the roots and the nearby planar regions increase gradually to approach the failure limit of a-Si thin film (~50 GPa) [45], the stress accumulated in the out-of-plane sections, that is, in the middle and on the top of the protruded radial junctions, are 2 and 4 orders of magnitude lower. This implies that the out-of-plane radial junction segments can be very well separated and protected from the stress concentrated on the bottom layer. More importantly, the mutual crossing radial junctions, as witnessed in Fig. 2a, can provide unique resilient and convenient 3D current pathways to extract the photo-carriers selectively from the active top segments that experience very little stress even under large bending. Finally, it is also important to note that the radial junctions on AF samples with standard EVA polymer encapsulation, where the thin film is sandwiched in the neutral strain plane, demonstrate an excellent robustness and flexibility that can sustain more than 200 times mechanical bending to 20 mm radius of curvature while retaining 80% PCE.

Compared to the flexible thin film solar cells reported in the literature and summarized in Table 1, the 3D construction of RJ solar cells directly upon the supermarket-available AF substrates can spare the use of extra surface texturing materials, which are usually accomplished by sacrificial etching into a thick TCO layer (for example, from 4 μm thick to 1.5–2 μm in conventional a-Si:H thin film solar cells) upon planar or AAO (anodized aluminum oxide) nano patterns [27,28]. More importantly, the SiNWs serving as firmly anchor sites to host the a-Si:H thin film and make it possible to deposit thin film solar cells directly upon the very cheap, soft and reflective AF surface. This removes the need for Ag or TCO as back reflector, buffer, and protection layers. Importantly, a strong light trapping performance has been well preserved among the 3D-RJs on AF solar cells, which help to achieve a relatively high J_{sc} output of 14.2 mA/cm^2. Combining the reasonable V_{oc} and overall PCE performances with a lightweight and flexible AF substrate, a record high PTW ratio of ~1300 W/kg has been achieved, which represents an important benefit for deploying flexible, portable and wearable electronics.

In addition, it is noteworthy that the possibility of a robust and

Table 1
Comparison of this work to the flexible a-Si:H solar cells reported in the literature.

Flexible a-Si:H thin film solar cells	Bending test	Substrate/thickness (μm)	Texturing technique	Back reflector/diffusion barrier	V_{OC} (V)	Jsc (mA/cm^2)	PCE %	Power-to -weight ratio (W/kg)	Reference
SS/AZO/Ag n-i-p a-Si:H/TTO	No data	SS/100	Ag (300 nm) by sputtering @500 °C	By Ag/AZO	0.93	13.36	7.6	~97*	[18]
SS/Al-Ag/Ag/ZnO:Ga/p-i-n a-Si:H/ZnO:Ga	No data	SS/125	Ag(150 nm)-Al(150 nm) alloy by sputtering & EBE	Al-Ag & Ag/ ZnO:Ga	0.843	13.98	8.44	~87*	[20]
PEN/Cr/ZnO NWs/p-i-n a-Si:H/AZO	Bent to local radius of ~6 mm	PEN/100	By 3D ZnO NWs	Cr/no	0.60	14.2	4	~80*	[21]
Al/Ag/AZO/n-i-p a-Si:H/ITO	Bent to local radius of ~1 cm*	Al/250	By AAO patterns formed in Al layer	Ag/AZO	~0.87	~13.6	~6.0	~88*	[27]
Al/Ag/ZnO:B/n-i-p a-Si:H/AZO	No data	Al/250	By AAO patterns formed in Al layer	Ag/ZnO:B	0.89	12.8	7.11	105*	[28]
PI/Al/ZnO or Ni/n-μc-Si:H i-p/TCO	No data	PI/100	By ZnO or Ni surface roughness	AZO or Ni/AZO or Ni	0.81	9.6	4.8	200	[5]
PI/Al/n-i a-Si p-a-SiC/TCO	Bent to local radius of 5 mm	PI/100	no	Al foil on PI/no	6.5	1.56	5.74	340	[6]
Al foil/p-SiNWs-i-n a-Si:H/ITO/Ag	Bent to local radius of 5 mm	Al foil/15	By 3D p-SiNWs	Al foil/no	0.71	14.2	5.6	1382	This work

* Estimated data according to figures and descriptions in references.

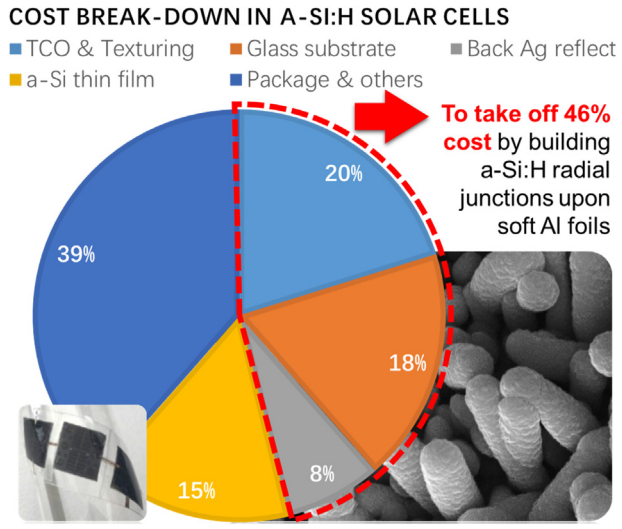

Fig. 6. The fabrication cost reduction by ~46% via 3D radial junction construction upon ultra-thin aluminum foils, compared to those in conventional a-Si:H module processing, while the bottom right and the left insets show the SEM image of the as-grown radial junctions on AF substrate and the photo image of a strip of encapsulated flexible RJ@AF cells wrapped around a small tube, respectively.

scalable construction of 3D-RJs directly upon the AF substrates brings in also an exciting opportunity to reduce the fabrication cost of a-Si:H modules by a large amount. Though a large scale verification of this strategy falls beyond the scope of this work, it is still reasonable, and also very instructive, to estimate the cost-reduction potential of this 3D-RJ@AF strategy. As schematized in Fig. 6, the cost breakdown of conventional planar a-Si:H thin film solar cells usually consists of the portions of TCO & Texturing (20%), glass substrate (20%), back Ag-reflector (8%) and a-Si thin films (15%), and package & others (39%) [46–50]. Because the AF is very cheap and highly reflective, almost as good as Ag layer in visible range, and the strong light trapping performance of 3D-RJs can help to remove the needs for extra TCO texturing structure and the back-reflection Ag coating layer, the fabrication cost of the a-Si:H 3D-RJs@AF solar cells could be greatly reduced to only 56% of the original cost. This significant cost reduction, combined with high flexibility and very high PTW performance, will help to promote the a-Si:H thin film technology to serve as a very competitive solution for high power-to-cost flexible photovoltaics.

4. Conclusions

In conclusion, we have demonstrated a robust 3D RJ flexible solar cells, built directly on ultra-thin AF of 15 μm thick, and achieved with very high PTW ratio performance of 1382 W/kg. The high flexibility and robust mechanical properties, even under large bending to local radii < 5 mm, are attributed to the unique 3D construction of radial junction units upon discrete SiNWs, which were grown and firmed rooted in the soft AF substrate. More importantly, without the need for a bottom TCO contact/texturing, nor for a back-reflection silver coating, the fabrication cost of a-Si:H solar cells can be largely reduced by ~46%. These results thus indicate a very promising new strategy to establish high performance flexible photovoltaics, catering to the needs of high flexibility, robustness, low-cost and high PTW performances in the booming portable and wearable electronics marketplace.

Acknowledgements

The authors acknowledge the financial support from the National Key Research and Development Program of China grants under Nos. 2016YFA0202102 and 2017YFA0205003, the National Natural Science Foundation of China (NSFC) under No. 61674075, the Jiangsu Excellent Young Scholar Program under No. BK20160020, the Scientific and Technological Support Program in Jiangsu province under No. BE2014147-2, Jiangsu Shuangchuang Team's Personal Program and the Fundamental Research Funds for the Central Universities. The authors also thanks *Trina Solar Ltd.* for the aids in solar cell encapsulation.

References

[1] Y. Li, Y.A. Samad, T. Taha, G. Cai, S.-Y. Fu, K. Liao, ACS Sustain. Chem. Eng. 4 (2016) 4288–4295.
[2] A.M. Zamarayeva, A.E. Ostfeld, M. Wang, J.K. Duey, I. Deckman, B.P. Lechêne, G. Davies, D.A. Steingart, A.C. Arias, Sci. Adv. (2017) e1602051.
[3] F. Fondjo, D.S. Lee, C. Howe, W.-H. Yeo, J.-H. Kim, IEEE 67th Electronic Components and Technology Conference, 2017, pp. 780-785.
[4] H. Cai, D. Zhang, Y. Xue, K. Tao, Sol. Energy Mater. Sol. Cells 93 (2009) 1959–1962.
[5] H. Nishiwaki, K. Uchihashi, K. Takaoka, M. Nakagawa, H. Inoue, A. Takeoka, S. Tsuda, M. Ohnishi, Sol. Energy Mater. Sol. Cells 37 (1995) 295.
[6] E. Findeisen, R.H.H. Tjokropranoto, J. Rijnenberg, J. Lenssen, A. Reinders, IEEE (2016) 2715–2717.
[7] M.P. Gaj, Georgia Institute of Technology, 2016.
[8] P. Docampo, J.M. Ball, M. Darwich, G.E. Eperon, H.J. Snaith, Nat. Commun. 4 (2013) 2761.
[9] J.H. Heo, M.H. Lee, H.J. Han, B.R. Patil, J.S. Yu, S.H. Im, J. Mater. Chem. A 4 (2016) 1572–1578.
[10] J.H. Heo, D.H. Shin, M.H. Jang, M.L. Lee, M.G. Kang, S.H. Im, J. Mater. Chem. A 5 (2017) 21146–21152.
[11] Y. Li, L. Meng, Y.M. Yang, G. Xu, Z. Hong, Q. Chen, J. You, G. Li, Y. Yang, Y. Li, Nat. Commun. 7 (2016) 10214.
[12] A.B. Roy, S. Das, A. Kundu, C. Banerjee, N. Mukherjee, Phys. Chem. Chem. Phys. 19 (2017) 12838–12844.
[13] M. Sharma, P.R. Pudasaini, F. Ruiz-Zepeda, D. Elam, A.A. Ayon, ACS Appl. Mater. Interfaces 6 (2014) 4356–4363.
[14] R.E.I. Schropp, M. Zeman, Springer science + business media, LLC, 1957.
[15] A.G. Aberle, Thin Solid Films 517 (2009) 4706–4710.
[16] M. Pagliaro, R. Ciriminna, G. Palmisano, ChemSusChem 1 (2008) 880–891.
[17] D.E. Carlson, C.R. Wronski, Appl. Phys. Lett. 28 (1976) 671–673.
[18] A.V. Shah, H. Schade, M. Vanecek, J. Meier, E. Vallat-Sauvain, N. Wyrsch, U. Kroll, C. Droz, J. Bailat, Prog. Photovolt.: Res. Appl. 12 (2004) 113–142.
[19] J.-S. Cho, S. Baek, J.C. Lee, Sol. Energy Mater. Sol. Cells 95 (2011) 1852–1858.
[20] Dong Zhanga, Miroslav Petrovb, Doriana Dimova-Malinovskab, Maarten Dörenkämpera, Klaas Bakkera, Ruud Schroppa, W. Soppea, in: Proceedings of the 29th European Photovoltaic Solar Energy Conference and Exhibition, 2014.
[21] K.H. Jung, S.J. Yun, S.H. Lee, Y.J. Lee, K.-S. Lee, J.W. Lim, K.-B. Kim, M. Kim, R.E.I. Schropp, Sol. Energy Mater. Sol. Cells 145 (2016) 368–374.
[22] M.K. Pathirane, W.S. Wong, Small 12 (2016) 2554–2558.
[23] K.-B. Kim, Appl. Sci. Converg. Technol. 26 (2017) 16–19.
[24] S. Cottrino, P. Viviès, D. Fabrègue, E. Maire, Acta Mater. 81 (2014) 98–110.
[25] S. Kao-Walter, Blekinge Inst. Technol. Res. Rep. 09 (2001).
[26] Q. Lin, L. Lu, M.M. Tavakoli, C. Zhang, G.C. Lui, Z. Chen, X. Chen, L. Tang, D. Zhang, Y. Lin, P. Chang, D. Li, Z. Fan, Nano Energy 22 (2016) 539–547.
[27] H. Xiao, J. Wang, H. Huang, L. Lu, Q. Lin, Z. Fan, X. Chen, C. Jeong, X. Zhu, D. Li, Nano Energy 11 (2015) 78–87.
[28] H. Huang, L. Lu, J. Wang, J. Yang, S.-F. Leung, Y. Wang, D. Chen, X. Chen, G. Shen, D. Li, Z. Fan, Energy Environ. Sci. 6 (2013) 2779–3100.
[29] C. Zhang, Y. Song, M. Wang, M. Yin, X. Zhu, L. Tian, H. Wang, X. Chen, Z. Fan, L. Lu, D. Li, Adv. Funct. Mater. 27 (2017) 1604720.
[30] Robert A. Street, William S. Wong, C. Paulson, Nano Lett. 9 (2009) 3494–3497.
[31] R.A. Street, P. Qi, R. Lujan, W.S. Wong, Appl. Phys. Lett. 93 (2008) 163109.
[32] P.-J. Alet, L. Yu, G. Patriarche, S. Palacin, P. Roca i Cabarrocas, J. Mater. Chem. 18 (2008) 5187.
[33] L. Yu, P.J. Alet, G. Picardi, I. Maurin, P.R. Cabarrocas, Nanotechnology 19 (2008) 485605.
[34] A. Belaidi, T. Dittrich, D. Kieven, J. Tornow, K. Schwarzburg, M. Lux-Steiner, Phys. Status Solidi (RRL) - Rapid Res. Lett. 2 (2008) 172–174.
[35] M. Krunks, A. Katerski, T. Dedova, I. Oja Acik, A. Mere, Sol. Energy Mater. Sol. Cells 92 (2008) 1016–1019.
[36] P. Ghamgosar, F. Rigoni, S. You, I. Dobryden, M.G. Kohan, A.L. Pellegrino, I. Concina, N. Almqvist, G. Malandrino, A. Vomiero, Nano Energy 51 (2018) 308–316.
[37] J. Cui, U.J. Gibson, J. Phys. Chem. C. 114 (2010) 6408–6412.
[38] M. Foldyna, L. Yu, P. Roca i Cabarrocas, Sol. Energy Mater. Sol. Cells 117 (2013) 645–651.
[39] L. Yu, S. Misra, J. Wang, S. Qian, M. Foldyna, J. Xu, Y. Shi, E. Johnson, P.R. Cabarrocas, Sci. Rep. 4 (2014) 4357.
[40] R.S. Wagner, W.C. Ellis, Appl. Phys. Lett. 4 (1964) 89–90.
[41] S. Misra, L. Yu, M. Foldyna, P. Roca i Cabarrocas, Sol. Energy Mater. Sol. Cells 118 (2013) 90–95.
[42] L. Yu, B. O'Donnell, M. Foldyna, P. Roca i Cabarrocas, Nanotechnology 23 (2012) 194011.
[43] L. Yu, L. Rigutti, M. Tchernycheva, S. Misra, M. Foldyna, G. Picardi, P. Roca i Cabarrocas, Nanotechnology 24 (2013) 275401.
[44] O. Keles, M. Dundar, J. Mater. Process. Technol. 186 (2007) 125–137.

[45] S. Wagner, H. Gleskova, I-C. Cheng, J.C. Sturm, Z. Suo, Wiley-SID Series in Display Technology, in: G.P. Crawford (Ed.), Flexible Flat Panel Displays, John Wiley & Sons, Ltd., 2005, p. 264 1433.
[46] A. Terakawa, Sol. Energy Mater. Sol. Cells 119 (2013) 204–208.
[47] A.V. Shah, H. Schade, M. Vanecek, J. Meier, E. Vallat-Sauvain, N. Wyrsch, U. Kroll, C. Droz, J. Bailat, Prog. Photovolt. Res. Appl. 12 (2004) 113–142.
[48] M. Konagai, Jpn. J. Appl. Phys. 50 (2011) (030001-030001-030012).
[49] A. Luque, S. Hegedus, Handbook of Photovoltaic Science and Engineering, 2nd ed., (2011).
[50] R.R. Arya, D.E. Carlson, Prog. Photovolt. Res. Appl. 10 (2002) 69–76.